RSC Advances

Synthesis, characterization, and adsorption properties of ionic liquid-modified hypercrosslinked polystyrene resin

Journal:	*RSC Advances*
Manuscript ID:	RA-ART-05-2015-008273.R2
Article Type:	Paper
Date Submitted by the Author:	23-Jul-2015

Complete List of Authors:	Wu, Xiaoyu; Lanzhou Institute of Chemical Physics, Chinese Academy of Sciences, Key Laboratory of Chemistry of Northwestern Plant Resources and Key Laboratory for Natural Medicine of Gansu Province; University of Chinese Academy of Sciences, Graduate University of the Chinese Academy of Sciences Liu, Yi; Lanzhou Institute of Chemical Physics, Chinese Academy of Sciences, Key Laboratory of Chemistry of Northwestern Plant Resources and Key Laboratory for Natural Medicine of Gansu Province; Lanzhou Institute of Chemical Physics, Chinese Academy of Sciences, Centre of Resource Chemical and New Material Liu, Yongfeng; Lanzhou Institute of Chemical Physics, Chinese Academy of Sciences, Key Laboratory of Chemistry of Northwestern Plant Resources and Key Laboratory for Natural Medicine of Gansu Province; Lanzhou Institute of Chemical Physics, Chinese Academy of Sciences, Centre of Resource Chemical and New Material Di, Duolong; Lanzhou Institute of Chemical Physics, Chinese Academy of Sciences, Key Laboratory of Chemistry of Northwestern Plant Resources Guo, Mei; Gansu College of Traditional Chinese Medicine, Department of Pharmacy Zhao, Lei; Gansu College of Traditional Chinese Medicine, Key Laboratory of Chemistry and Quality for Traditional Chinese Medicines of the College of Gansu Province

RSC Advances

ARTICLE

Synthesis, characterization, and adsorption properties of ionic liquid-modified hypercrosslinked polystyrene resin

Received 00th January 20xx,
Accepted 00th January 20xx

DOI: 10.1039/x0xx00000x

www.rsc.org/

Xiaoyu Wu[a,b], Yi Liu[a,c], Yongfeng Liu[a,c], Duolong Di[a,c*], Mei Guo[d] and Lei Zhao[e]

Abstract: A series of ionic liquid modified hypercrosslinked polystyrene resins are synthesized by adding different quantities of imidazole in the Friedel–Crafts reaction. The resins are characterized by nitrogen adsorption/desorption, Fourier transform infrared spectroscopy, elemental analysis and scanning electron microscopy. The adsorption properties of (−)-epigallocatechin gallate and (−)-epicatechin are investigated and compared with macroporous adsorption resins Seplite D101 and Seplite AB-8. The (−)-epigallocatechin gallate and (−)-epicatechin uptakes on HP-IL16 are remarkably larger than those of macroporous adsorption resins Seplite D101 and Seplite AB-8. The maximum adsorption capacity of HP-IL16 are up to 73.1 mg/g for (−)-epigallocatechin gallate and 93.0 mg/g for (−)-epicatechin. The adsorption isotherms are best described by the Langmuir model, and their adsorption kinetics follow the pseudo-second-order kinetic equation and intra-particle diffusion model. Analysis of the adsorption mechanism suggest that the synergistic effect of the specific surface area,

[a] Key Laboratory of Chemistry of Northwestern Plant Resources and Key Laboratory for Natural Medicine of Gansu Province, Lanzhou Institute of Chemical Physics, Chinese Academy of Sciences, Lanzhou 730000, China. E-mail address: didl@licp.cas.cn; Tel: +86-931-496-8248; fax: +86-931-496-8248
[b] Graduate University of the Chinese Academy of Sciences, Beijing 100049, China
[c] Centre of Resource Chemical and New Material, Lanzhou Institute of Chemical Physics, Chinese Academy of Sciences, Qingdao 266100, China
[d] Department of Pharmacy, Gansu College of Traditional Chinese Medicine, Lanzhou 730000, China
[e] Key Laboratory of Chemistry and Quality for Traditional Chinese Medicines of the College of Gansu Province, Gansu College of Traditional Chinese Medicine, Lanzhou, 730000, China

molecular sieving effect, and multiple adsorption interactions are the driving forces of adsorption. The resin is reusable and presents a good desorption rate. Based on these results, this study opens up the possibility of synthesizing ionic liquid modified hypercrosslinked polymeric resins for purification of catechin from herbal plants.

Introduction

Numerous traditional methods, such as precipitation, filtration, solvent extraction, solid phase extraction and chromatography, for extracting the active compounds in the herbal plants have been applied[1,2]. In recently years, polymeric resins have attracted a great deal of attention because of their structural diversity, favorable physicochemical stability and easy regeneration[3-6]. In particular, adsorbents based on hypercrosslinked polystyrene are widely investigated[7]. Hypercrosslinked polystyrene was first introduced in the 1970s by Davankov and Tsyurupa[8,9]. Hypercrosslinked resins are generally prepared from a linear polystyrene or low-crosslinked poly(styrene-co-divinylbenzene) using a bifunctional crosslinking agent and a Friedel–Crafts catalyst. At present, applications of hypercrosslinked polymers include the separation of organic compounds from gaseous or liquid phase[10,11], gas storage material[12], and ion exchange resins[13]. However, only limited studies on hypercrosslinked polymeric resin as adsorbents for purification of active ingredients from herbal plants have been conducted[14].

Hypercrosslinked polymeric resins possess high specific surface area and pore size distribution in the micropore and mesopore regions. However, given the high hydrophobicity of the matrix, adsorption selectivity toward polar aromatic compounds is relatively low. Low selectivity could be overcome by introducing polar functional groups onto the resin network. Wang et al.[15] synthesized aniline-functionalized hypercrosslinked polystyrene resins and investigated adsorption selectivity toward salicylic acid. Vinodh et al.[16] fabricated a novel microporous hypercross-linked conjugated quinonoid chromophores with broad light absorption and CO_2 sorption characteristics. Li et al.[17] studied sulfonic acid-modified microporous hypercrosslinked polymers as a high-capacity adsorbent for toxic metal ions.

This work aims to prepare hypercrosslinked adsorbents functionalized with ionic liquids (ILs) and have large surface area, polar groups, and bimodal distribution of pore sizes for separation and purification of small-molecule active ingredients from herbal plants. In our previous studies, ILs are used for the first time as adsorbent to modify macroporous adsorption resins and purify flavonoids from *Hippophae rhamnoides* L. leaves[18]. ILs can be defined as a class of ionic and non-molecular solvents composed of large organic cations and small anions[19,20]. ILs are primarily advantageous because of their tunability, low melting point, and wide range of solubility and viscosity. In addition, polymeric adsorbent

functioned with ILs has been synthesized to enhance the adsorption selectivity of catechin[21].

Catechins are the most abundant components in tea polyphenolic flavonoids, comprising (−)-epigallocatechin gallate (EGCG), (−)-epicatechin gallate (ECG), (−)-epigallocatechin (EGC), and (−)-epicatechin (EC). Catechins has also demonstrated beneficial effects in studies of cancer preventive effects, possesses antioxidant activity, as well as activities against diabetes[22,23]. Given these biological activities, extraction and purification of catechins have been significantly challenging in chemistry.

Considering our research interests and previous work, we synthesized a series of imidazole-modified hypercrosslinked resins from low crosslinked chloromethylated polystyrene by adding different quantities of imidazole. EGCG and EC were selected as model catechin compounds for the sorption study. The adsorption selectivity of resins toward EGCG and EC were confirmed by batch adsorption. The most promising resin, HP-IL16, was selected for detailed experimental studies for adsorption. Its adsorption kinetics and equilibrium behavior compared with macroporous adsorption resins Seplite D101 and Seplite AB-8 were investigated. Moreover, the adsorption thermodynamic parameters were analyzed and the adsorption mechanism was expounded.

Experimental

Synthesis of ionic liquid-modified hypercrosslinked resins

As described in Scheme 1, ILs modified hypercrosslinked polystyrene resins were fabricated by two continuous steps[24]. First, 40 g of chloromethylated polystyrene beads was swollen in 120 mL of nitrobenzene overnight. Under mild mechanical stirring, 4 g of anhydrous zinc chloride was added into the reaction flask at 323 K. After the added zinc chloride was completely dissolved, the reaction mixture was evenly heated to 388 K within 1 h using linear temperature program with gradients of 1°C/55 seconds. The reaction was carried out continuously at 388 K for 10 h. After the reaction, the beads were washed with acetone, 1% hydrochloric acid (v/v), and de-ionized water until neutral; extracted with ethanol in Soxhlet apparatus for 12 h; and then dried at 323 K in vacuum. The hypercrosslinked polystyrene resin, HP-IL, was obtained.

Second, 10 g of the HP-IL resin was swollen in 135 mL of N,N-dimethylformamide for 12 h.

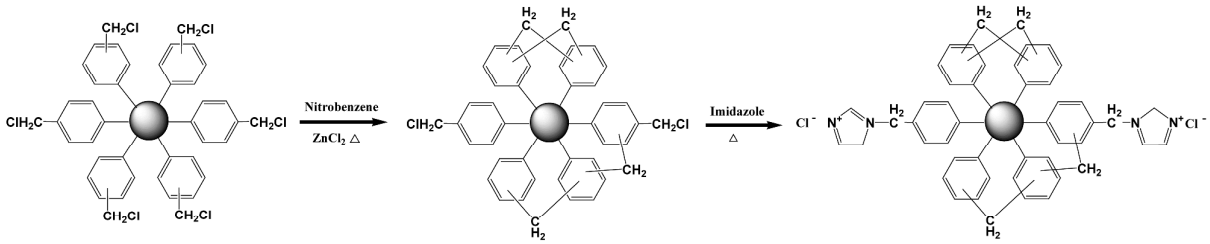

Scheme 1 Schematic illustration for the synthesis of ionic liquid-modified hypercrosslinked polystyrene resin

Approximately 5 g of sodium hydroxide and different dosages of imidazole (4%, 8%, 12%, 16%, and 20% relative to chloromethylated polystyrene, w/w) were added into the flask. After holding for about 12 h at 343 K, the polymeric beads were rinsed with distilled water, extracted with ethanol for 12 h, and dried at 323 K in vacuum. The imidazole-modified hypercrosslinked polystyrene resins, namely, HP-IL04, HP-IL08, HP-IL12, HP-IL16, and HP-IL20, were synthesized accordingly.

Characterization of the resins

Chlorine content determination was carried out with the Volhard method[25]. The pore structure of the resins was determined by nitrogen adsorption and desorption isotherms at 77 K using a Micromeritics ASAP 2020 automatic surface area. The infrared spectra of the resins were obtained with a Fourier transform infrared (FTIR) spectrophotometer by potassium bromide technique in the range of 400 cm^{-1} to 4000 cm^{-1}. Elemental analysis of the resins was performed with a Vario EL elemental analysis system. The morphology of the resins were carried out by JSM--6701 scanning electron microscopy (SEM).

Results and discussion

Characteristics of the resins

As listed in Table 1, the chlorine content of HP-IL sharply decreased from 4.56 mmol/g to 2.01 mmol/g, indicating that the chlorine of chloromethylated PS was consumed in the Friedel–Crafts reaction. The chlorine contents of the HP-IL series resins were further reduced with the increment of added imidazole quantity, indicating that the uploading amounts of imidazole on the resins were different. HP-IL20 should possess the highest uploading amount, while HP-IL04 may own the least. These results were in agreement with the elemental analysis, wherein the nitrogen content of HP-IL, HP-IL04, HP-IL08, HP-IL12, HP-IL16, and HP-IL20 was 0%, 1.22%, 1.68%, 2.05%, 2.32%, 2.77%, and 3.13%, respectively. These results also demonstrated that imidazole was successfully uploaded on the surface of the resins.

The BET surface area of HP-IL sharply increased compared with that of chloromethylated

Table 1 Physical properties of the ionic liquid-modified hypercrosslinked polystyrene resins.

	HP-IL	HP-IL04	HP-IL08	HP-IL12	HP-IL16	HP-IL20
BET surface area (m^2/g)	888.8	854.1	845.5	832.6	826.9	815.3
Langmuir surface area (m^2/g)	1188.7	1141.5	1129.2	1118.6	1104.7	1087.9
t-Plot micropore surface area (m^2/g)	505.1	503.6	502.3	494.0	488.4	481.5
Pore volume (cm^3/g)	0.70	0.66	0.67	0.64	0.65	0.62
t-Plot micropore volume (cm^3/g)	0.23	0.22	0.23	0.22	0.22	0.22
Average pore width (nm)	3.17	3.15	3.13	3.09	3.13	3.06
Particle size (mm)	0.2−0.3	0.2−0.3	0.2−0.3	0.2−0.3	0.2−0.3	0.2−0.3
Chlorine content (mmol/g)	2. 01	1.59	1.32	1.16	0.98	0.95
Functional degree (mmol/g)	-	0.42	0.69	0.85	1.03	1.06

PS, which may be attributed to the large quantity of methylene crosslinking bridges formed between the polystyrene chains in the Friedel–Crafts reaction[27]. In addition, the micropore surface area is more than half of the whole BET surface area, implying that micropores perform an important function in the pore structures. After nucleophilic substitution reaction, the BET surface area of HP-IL series resins gradually reduced, which may be attributed to the partial destruction of the high degree of crosslinking by uploading imidazole on the resins. The pore volume and t-plot micropore volume of HP-IL series resins only slightly changed, which may be due to the introduced functional groups modifying the surface of the adsorbent, resulting in less impact on the pore volume and t-plot micropore volume.

The nitrogen adsorption capacity on HP-IL and HP-IL16 were substantially larger than that on chloromethylated PS (see Fig. 1), indicating the greater BET surface area of HP-IL and HP-IL16 with respect to chloromethylated PS. The nitrogen adsorption–desorption isotherms of the HP-IL series resins are demonstrated in Fig. S1. All isotherms show the same tendency as HP-IL16. The initial part of the adsorption isotherms at lower

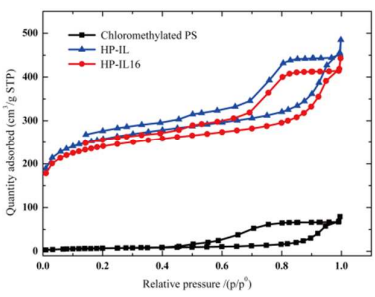

Fig.1 N_2 adsorption and desorption isotherms of the chloromethylated PS, HP-IL, HP-IL16.

relative pressure (P/P_0) below 0.05, under which nitrogen uptake increases sharply with the increment of relative pressure, proves the existence of micropore structure. Moreover, the visible hysteresis loop of the desorption isotherm indicates that mesopores are also present[28]. These results are in agreement with the pore diameter distribution in Fig. 2. Evidently, micropores/mesopores provide a main contribution to the whole BET surface area. The same trend of the pore diameter distribution of HP-IL series resins are demonstrated in Fig. S2. The micropore and mesopores range of the HP-IL series resins suggest its function as a good adsorbent for the adsorption of small-molecule compounds.

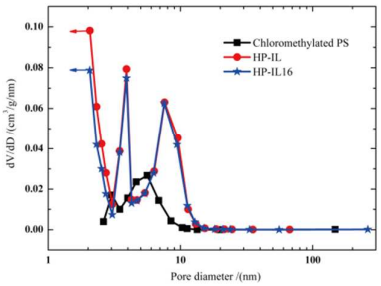

Fig.2 The pore diameter distribution of the chloromethylated PS, HP-IL, HP-IL16.

The image in Fig. 3 shows the FTIR spectra of chloromethylated PS, HP-IL, and HP-IL16. The FTIR spectra of the HP-IL series resins present the same trend as HP-IL 16 (see Fig. S3). The spectrum of chloromethylated PS characterizes its polystyrene-type structure based on the representative vibrations at 3019, 2930, 1603, 1510, and 1448 cm^{-1}[21]. Two strong representative

peaks at 1265 and 669 cm^{-1} were assigned to the adsorption of vibration by $-CH_2Cl$[29]. After Friedel–Crafts reaction, two representative strong vibrations of $-CH_2Cl$ groups at 1265 and 669 cm^{-1} are considerably weakened, in accordance with the sharp decrease in chlorine content. This result suggested that a hypercrosslinked resin was successfully formed. After the nucleophilic substitution reaction, the peak at 1265 and 669 cm^{-1} were further reduced, while three other vibrations with frequencies at 1365, 1716, and 1564 cm^{-1} were presented, which can be attributed to the characteristic frequency of imidazolium groups[30,31]. As a result, introduction of imidazole to the surface of the hypercrosslinked resin was achieved successfully.

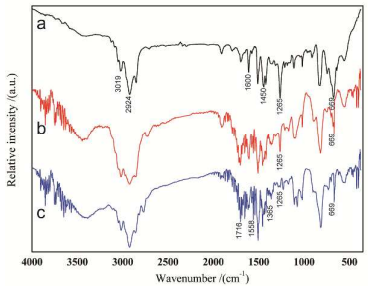

Fig.3 FTIR spectra of the chloromethylated PS (a), HP-IL (b), HP-IL16 (c).

Fig. 4 presents the SEM images of the three polymeric resins. It can be seen that their morphologies are quite different from each other. The chloromethylated PS shows a relatively smooth and compact surface with many particle. Meanwhile, the image indicated that the chloromethylated PS owned less porous structure. The HP-IL displays a more hierarchical porous structure after Friedel-Crafts reaction. It can be seen clearly that the surface of HP-IL16 is the roughest among three polymeric resins, which is probably induced by the chemical modification of the surface. This results are consistent with the BET surface area of three polymeric resins. The SEM images intuitively reflect the reaction process.

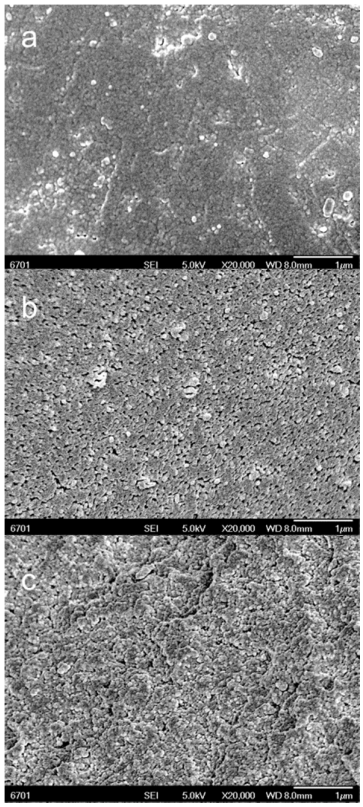

Fig. 4 SEM images of the chloromethylated PS (a), HP-IL (b), HP-IL16 (c).

Adsorption selectivity

The adsorption capacities of EGCG and EC on HP-IL, HP-IL04, HP-IL08, HP-IL12, HP-IL16, and HP-IL20 are compared in Fig. 5. Evidently, the EGCG and EC uptakes initially increased, and then decreased with the increment of imidazole doze. After uploading imidazole on the resins, the BET surface area decreased, whereas the polarity of resins increased. The increased polarity may lead to

an increased adsorption capacity toward polar compounds. The adsorption capacity of EGCG and EC on HP-IL16 was the largest among the six resins; hence, HP-IL16 was employed as a specific polymeric adsorbent in this study.

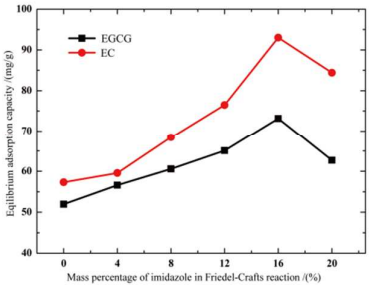

Fig.5 Comparison of equilibrium EGCG and EC uptakes on HP-IL04, HP-IL08, HP-IL12, HP-IL16 and HP-IL20.

Macroporous adsorption resins Seplite D101 and Seplite AB-8 are the best common commercial polymeric resins. Thus, the adsorption isotherms of HP-IL16 toward EGCG and EC were compared with macroporous adsorption resins Seplite D101 and Seplite AB-8 at the same experimental condition. As shown in Fig. 6, the adsorption capacity onto HP-IL16 was evidently larger than that onto macroporous adsorption resins Seplite D101 and Seplite AB-8. The larger adsorption capacity of HP-IL16 may result from the specific surface area, polarity, and the pore diameter between the HP-IL16 and EGCG, and EC. These interactions act synergistically with one another in the adsorption process.

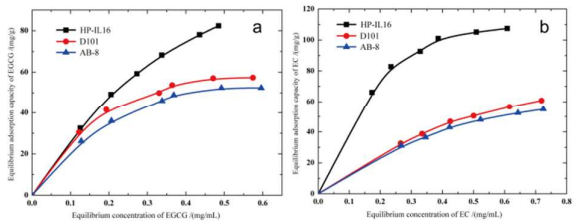

Fig.6 Adsorption isotherms of EGCG (a) and EC (b) on D101, AB-8, and HP-IL16 at 288 K..

Kinetic experiments

Adsorption kinetics is beneficial in predicting adsorption rate and provides important information for designing and modeling the adsorption process. The adsorption kinetics curves for EGCG and EC on macroporous adsorption resins Seplite D101, Seplite AB-8, and HP-IL16 at 288 K are displayed in Fig. 7. As shown in the figure, the adsorption capacity of EGCG and EC on HP-IL16 is the highest among the resins. The required time for the adsorption of EGCG and EC onto HP-IL16 from beginning to equilibrium is about 600 min, which is considerably longer than those for macroporous adsorption resins Seplite D101 and Seplite AB-8. This result implies that macroporous adsorption resins Seplite D101 and Seplite AB-8 possesses the highest adsorption rate, which may be due to the different pore structures.

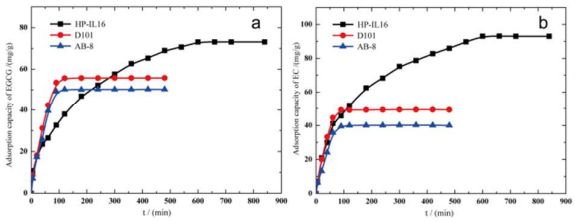

Fig.7 Adsorption kinetic curves of EGCG (a) and EC (b) on D101, AB-8 and HP-IL16 at 288 K

Three common kinetic models, namely, pseudo-first-order, pseudo-second-order, and intra-particle diffusion, are applied for goodness-of-fit to the experimental data to further explain the adsorption mechanisms. The pseudo-first-order equation can be represented as follows[32]:

$$\ln\left(q_e - q_t\right) = -k_1 t + \ln q_e$$

The pseudo-second-order equation used was as follows[32]:

$$\frac{t}{q_t} = \frac{1}{q_e} t + \frac{1}{k_2 q_e^{\,2}}$$

The intra-particle diffusion model can be arranged as follows[33]:

$$q_t = k_{id} t^{1/2} + C$$

where q_t and q_e are the adsorption capacity at contact time t and equilibrium, respectively. Parameters k_1 (1/min), k_2 [g/(mg min)], and k_{id} [mg/(g min$^{1/2}$)] are the rate constants of the pseudo-first-order, pseudo-second-order, and intra-particle diffusion models, respectively. The constant C (mg/g) represents the boundary layer thickness.

Plotting $ln\ (q_e - q_t)$ against t, t/q_t via t, and q_t versus $t^{1/2}$ produced straight line graphs. The fitted correlative parameters are summarized in Table 2. Notably, both pseudo-second-order equation and intra-particle diffusion equation are suitable for EGCG and EC adsorption on HP-IL16, while adsorption on macroporous adsorption resins Seplite D101 and Seplite AB-8 can only be fitted by the pseudo-second-order equation. This finding was deduced from the higher correlation coefficient values (R^2). In addition, the values of q_e for EGCG and EC were close to the experimental equilibrium capacity values, implying that the pseudo-second-order kinetic model could feasibly describe the adsorption process.

Intra-particle diffusion is the rate-limiting step for the adsorption of aromatic compounds onto hypercrosslinked resins from aqueous solutions[33]. The image in Fig. 8 shows the plot of q_t versus $t^{1/2}$ for adsorption on HP-IL16, exhibiting three portions. At the first stage, a linear relationship is observed and the straight lines pass through the origin, implying that the intra-particle diffusion is the rate-limiting step. At the second stage, plots of q_t versus $t^{1/2}$ also yield linear relationships but do not pass through the origin, revealing that multi-diffusion mechanisms are involved. At the third stage, adsorption reaches equilibrium, during which intra-particle diffusion starts to slow down because of the extremely low EGCG and EC concentrations left in solution.

Table 2 Kinetic parameters for adsorption of EGCG and EC onto MARs.

	pseudo-first-order equation			pseudo-second-order equation			intra-particle diffusion equation		
	k_1/(1/min)	q_e/(mg/g)	R^2	k_2/(g/mg min)	q_e/(mg/g)	R^2	k_{id}/(mg/g min$^{1/2}$)	C/(mg/g)	R^2
EGCG									
D101	0.0177	13.46	0.7488	0.0007	59.88	0.9954	2.12	19.07	0.6770
AB-8	0.0166	11.13	0.7478	0.0007	53.76	0.9948	1.92	17.09	0.6623
HP-IL16	0.0099	129.02	0.8492	0.0001	84.03	0.9811	2.70	7.43	0.9811
EC									
D101	0.0148	7.17	0.6998	0.0110	52.08	0.9965	1.68	20.71	0.5886
AB-8	0.0129	6.89	0.6433	0.0011	42.55	0.9952	1.44	15.44	0.6146
HP-IL16	0.0091	139.77	0.8341	0.0001	106.38	0.9941	3.43	10.37	0.9645

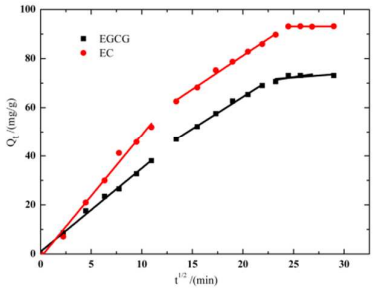

Fig.8 Correlations of q_t versus $t^{1/2}$ for the adsorption of EGCG and EC on HP-IL16 by intra-particle diffusion model.

Equilibrium adsorption

The equilibrium adsorption isotherms of EGCG and EC on HP-IL16 are obtained at 288, 298, and 308 K, respectively. The results are displayed in Fig. 9. Evidently, adsorption capacity increases with increasing concentrations of both EGCG and EC, and temperature. Adsorption is an endothermic process, indicating that high temperature is more favorable for adsorption.

Adsorption isotherms are useful in understanding adsorption mechanisms. Langmuir and Freundlich models are used to fit adsorption isotherms and describe the adsorption behavior. The Langmuir isotherm valid for monolayer adsorption on a surface containing a finite number of identified sites. The Langmuir isotherm equation is given by[34]:

$$\frac{C_e}{q_e} = \frac{K_L}{q_m} + \frac{C_e}{q_m}$$

The Freundlich model assumes that adsorption occurs at heterogeneous surfaces, which are characterized by sorption sites at different energies. The Freundlich isotherm equation could be expressed as follows[34]:

$$\ln q_e = \frac{1}{n}\ln C_e + \ln K_F$$

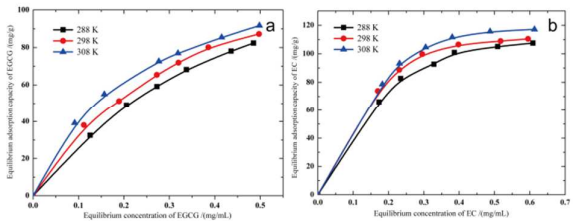

Fig. 9 Adsorption isotherms of EGCG (a) and EC (b) on HP-IL16 at the temperature of 288, 298, 308 K, respectively.

where C_e is the equilibrium concentration (mg/mL), q_e is the equilibrium adsorption capacity (mg/g), q_m is the maximum adsorption capacity (mg/g), K_L is a constant (L/mg), K_F is the parameter related to the adsorption energy [(mg/g)(L/mg)$^{1/n}$], and $1/n$ is the Freundlich characteristic constant.

The equilibrium data in Fig. 9 were fitted into these two isotherm models. The corresponding parameters of Langmuir and Freundlich models

Table 3 Langmuir isotherm parameters of EGCG and EC onto MARs.

		EGCG				EC			
		q_m/(mg/g)	K_L/(mg/mL)	R_L	R^2	q_m/(mg/g)	K_L/(mg/mL)	R_L	R^2
HP-IL16	288 K	172.41	0.53	0.43	0.9953	140.85	0.17	0.17	0.9909
	298 K	147.06	0.34	0.33	0.9918	134.14	0.15	0.16	0.9927
	308 K	129.87	0.22	0.24	0.9992	144.93	0.13	0.14	0.9902
D101	288 K	75.76	0.17	0.19	0.9926	123.46	0.72	0.47	0.9905
AB-8	288 K	73.53	0.21	0.23	0.9862	100.00	0.58	0.42	0.9906

were calculated and tabulated in Table 3 and Table S1. The results showed that the Langmuir model was more appropriate for describing the experimental data because of its highly dependable correlation coefficients. This result indicated homogeneous adsorption through a monolayer solid–liquid adsorption mechanism. The essential characteristics of the Langmuir isotherm can be expressed in terms of dimensionless constant (R_L), which is expressed by the following equation[35,36]:

$$R_L = \frac{1}{1 + C_0 / K_L}$$

According to the Langmuir theory, R_L values indicate the isotherm type. The isotherm type is unfavorable when $R_L > 1$, linear when $R_L = 1$, favorable when $0 < R_L < 1$, and irreversible when $R_L = 0$. The values of R_L for EGCG and EC at different temperatures ranged from 0 to 1, indicating adsorption of EGCG and EC on HP-IL16 is favorable.

Thermodynamic analysis

To obtain in-depth information on inherent energetic changes associated with the adsorption process, thermodynamics parameters, including adsorption Gibbs free energy ($\Delta G°$), adsorption enthalpy ($\Delta H°$), and adsorption entropy ($\Delta S°$), were calculated following a derivative of the van't Hoff equation[37]. The liquid-phase adsorption followed the Langmuir isotherm equation. The thermodynamic parameters can be calculated according to the following equations:

$$K = \frac{M}{K_L}$$

$$\Delta G° = -RT \ln K$$

$$\ln K = -\frac{\Delta H°}{RT} + \frac{\Delta S°}{R}$$

where K_L is the Langmuir isotherm constant (L/mg), M is the molecular weight of EGCG and EC (g/mol), T is the absolute temperature (K), and R is the ideal gas constant (J/mol K).

Using a linear plot between ln K against $1/T$, the adsorption enthalpy and entropy for the adsorption process could be obtained according to the slope and intercept of the plot. Among the data in Table 4, the values of $\Delta G°$ were all negative, indicating that the adsorption reaction was a spontaneous process. The positive values of $\Delta H°$ for HP-IL16 demonstrated an endothermic nature for this process. A temperature increase favors the adsorption process. The value of $\Delta S°$ for EGCG and EC were all positive, indicating that randomness at the solid–liquid interface increased during the adsorption process. Positive values of $\Delta S°$ were most likely attributed to the release of water molecules from EGCG and EC.

Adsorption mechanism

The image in Fig. 7 depicts that the adsorption capacity of EGCG and EC onto HP-IL16 is larger than those of macroporous adsorption resins Seplite D101 and Seplite AB-8. The adsorption capacity of EGCG on HP-IL16 increased from 55.7 (macroporous adsorption resins Seplite D101) and 50.2 mg/g (macroporous adsorption resins Seplite AB-8) to 73.1 mg/g. The BET surface areas of HP-

IL16, macroporous adsorption resins Seplite D101, and Seplite AB-8 are 826.9, 726.1, and 474.9 m^2/g, respectively. Compared with that of macroporous adsorption resins Seplite D101, the BET surface area of HP-IL16 increased by 13%, whereas the adsorption capacity of EGCG was enhanced by 31%. In other words, specific surface area does not play a crucial function. EGCG consists of epigallocatechin and gallate ester groups, implying that EGCG possesses higher diffusion resistance and slow diffusion rates. EGCG diffused into the pore of HP-IL6 with difficulty. Therefore, pore diameter matching is also insignificant. The HP-IL16 is a hypercrosslinked resin with an embedded polar imidazolium functional group. Owing to the imidazolium group, HP-IL16 can interact with EGCG through multiple interactions, including π–π interactions, ion–dipole interactions, electrostatic interactions, as well as hydrogen bonding. Therefore, polarity matching between HP-IL16 and EGCG is the main adsorption driving force for adsorption[38].

The adsorption capacity of EC on HP-IL16, macroporous adsorption resins Seplite D101, and Seplite AB-8 are 93.0, 49.3, and 40.1 mg/g, respectively. Compared with that of macroporous adsorption resins Seplite D101, the BET surface area of HP-IL16 increased by 13%, whereas the adsorption capacity of EC was enhanced by 88%. Hence, specific surface area is insignificant in adsorption. Polarity matching between HP-IL16 and EC also involved multiple π–π, ion–dipole, and electrostatic interactions, as well as hydrogen bonding. However, the structure of EC only includes epicatechin groups, implying a smaller number of multiple interaction sites. As a result, the polarity matching between HP-IL16 and EC plays a small role in adsorption capacity. The micropores/mesopores play a predominant role in the pore structure for HP-IL16, which is suitable for HP-IL16 and EC interaction through the pore filling mechanism. The results are in agreement with the intra-particle diffusion model. The structure of EC includes epicatechin groups, implying that EC presents lower diffusion resistance and rapid diffusion rates. EC more easily diffused into the pore of HP-IL6. In consequence, the pore diameter between the HP-IL16 and EC performs a leading function in the adsorption process, indicating a molecular sieving effect[39].

Table 4 Thermodynamics parameters for the adsorption of EGCG and EC onto HP-IL16.

Thermodynamics parameters	ΔG^0/(kJ/mol)			ΔH^0/(kJ/mol)	ΔS^0/(J/mol K)	R^2
	288 K	298 K	308 K			
EGCG	-16.2	-17.9	-19.6	32.4	168.7	0.9928
EC	-17.8	-18.8	-19.7	9.9	96.2	0.9916

Recycling ability of the resins

To test the reusability of the resins, the macroporous adsorption resins Seplite D101, Seplite AB-8, and HP-IL16 resins were used repeatedly for five times for continuous adsorption and desorption of EGCG and EC. After adsorption, 100 mL of methanol was applied as desorption reagent. Desorption efficiency was generally high (more than 90%). As shown in Fig. 10, the adsorption capacities of EGCG and EC on HP-IL16 was reduced by only 9.0% for EGCG and 8.3% for EC after five adsorption–desorption cycles, which demonstrated that the HP-IL16 resins exhibit good reusability with remarkable regeneration behaviors.

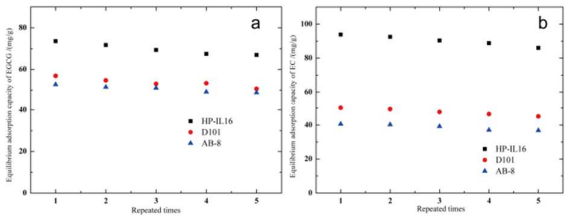

Fig. 10 Effect of the regeneration cycles on the adsorption capacity of EGCG (a) and EC (b) on the D101, AB-8 and HP-IL16 at 288 K.

Conclusions

A series of imidazolium-modified hypercrosslinked polystyrene resins, namely, HP-IL04, HP-IL08, HP-IL12, HP-IL16, and HP-IL20, were synthesized, and the obtained resins presented different BET surface areas and polarities. The adsorption capacity of EGCG and EC on resins initially increased, and then decreased with increasing quantity of imidazolium in the Friedel–Crafts reaction. HP-IL16 presented the largest adsorption capacity. The kinetic data could be fitted by pseudo second-order rate equation and intra-particle diffusion model. The Langmuir isotherm model was more suitable for fitting the equilibrium data than the Freundlich model. Thermodynamic parameters showed that adsorption is a spontaneous and an endothermic process. Analysis of the adsorption mechanism suggested that specific surface area, molecular sieving effect, and multiple adsorption interactions were the driving forces of the adsorption. These factors acted synergistically in the adsorption process. The resin could be completely desorbed by methanol, and the adsorption capacity of EGCG and EC on HP-IL16 decreased to approximately 91.0% and 91.7% after five adsorption–desorption cycles. The experimental results indicated the possibility of enhancing the adsorption capacity for catechin from herbal plants using imidazolium modified hypercrosslinked polystyrene resins.

Acknowledgments

The authors gratefully acknowledge the support of the National Natural Science Foundation of China (NSFC, no. 21374128) and the "Hundred Talents Program" of the Chinese Academy of Sciences for this work.

The authors declare no competing financial interest(s).

References

Review

1 Roger M. Smith, Before the injection-modern methods of sample preparation for separation

techniques-review, *J. Chromatogr. A.*, 2003, 1000, 3–27.

2 Yi Chen, Zhenpeng Guo, Xiaoyu Wang, Changgui Qiu, Sample preparation-review, *J. Chromatogr. A.*, 2008, 1184, 191–219.

3 M.E. León-González and L.V. Pérez-Arribas, Chemically modified polymeric sorbents for sample preconcentration, *J. Chromatogr. A.*, 2000, 902, 3–1.

4 S-H. Lin and R-S. Juang, Adsorption of phenol and its derivatives from water using synthetic resins and low-cost natural adsorbents: a review, *J. Environ. Manage.*, 2009, 90, 1336–1349.

5 G.W. Yang, H.Y. Han, C.Y. Du, Z.H. Luo and Y.J. Wang, Facile synthesis of melamine-based porous polymer networks and their application for removal of aqueous mercury ions, *Polymer*, 2010, 51, 6193–6202.

6 Q.P. Xiong, Q.H. Zhang, D.Y. Zhang, Y.Y. Shi, C.H. Jiang and X.J. Shi, Preliminary separation and purification of resveratrol from extract of peanut (*Arachis hypogaea*) sprouts by macroporous adsorption resins, *Food Chem.*, 2014, 145, 1–7.

7 Q.Q. Liu, Z. Tang, M.D. Wu, B. Liao, H. Zhou, B.L. Ou, .P. Yu, Z.H. Zhou and X.J. Li, Novel ferrocene-based nanoporous organic polymers for clean energy application, *RSC Adv.*, 2015, 5, 8933–8937.

8 S.V. Rogozhin, V.A. Davankov and M.P. Tsyurupa, Patent USSR 299165, 1969.

9 A. Tadim, V.A. Davankov and M.P. Tsyurupa, Structure and properties of porous hypercrosslinked polystyrene sorbents 'Styrosorb', *Pure Appl. Chern.*, 1989, 61, 1881–1888.

10 X. Yang, M. Yu, Y. Zhao, C. Zhang, X.Y. Wang and J-X. Jiang, Hypercrosslinked microporous polymers based on carbazole for gas storage and separation, *RSC Adv.*, 2014, 4, 61051–61055.

11 J.T. Wang, S. Xu, .F. Wang, R. Cai, C.X. Lv, W.M. Qiao, D.H. Long and L.C. Ling, Controllable synthesis of hierarchical mesoporous/microporous nitrogen-rich polymer networks for CO_2 and Cr(VI) ion adsorption, *RSC Adv.*, 2014, 4, 16224–16232.

12 Z.W. Tang, S.F. Li, W.N. Yang and X.B. Yu, Hypercrosslinked porous poly(styrene-co-divinylbenzene) resin: a promising nanostructure-incubator for hydrogen storage, *J. Mater. Chem.*, 2012, 22, 12752–12758.

13 P.A.G. Cormack, A. Davies and N. Fontanals, Synthesis and characterization of microporous polymer microspheres with strong cation-exchange character, *React. Funct. Polym.*, 2012, 72, 939–946.

14 Y. Li, R.F. Cao, X.F. Wu, J.H. Huang, S.G. Deng and X.Y. Lu, Hypercrosslinked poly(styrene-co-divinylbenzene) resin as a specific polymeric adsorbent for purification of berberine hydrochloride from aqueous solutions, *Chem. Eng. J.*, 2013, 400, 78–87.

15 X.M. Wang, X.J. Yuan, S. Han, H.W. Zha, X.C. Sun, J.H. Huang and Y-N. Liu, Aniline modified hypercrosslinked polystyrene resins and their adsorption equilibriums, kinetics and dynamics towards salicylic acid from aqueous solutions, *Chem. Eng. J.*, 2013, 233, 124–131.

16 R. Vinodh, P. Hemalatha, M. Ganesh, M.M. Peng, A. Abidov, M. Palanichamy, W. S. Cha and Hyun-T. Jang, Novel microporous hypercross-linked conjugated quinonoid chromophores with broad light absorption and CO_2 sorption characteristics, *RSC Adv.*, 2014, 4, 3668-3674.

17 B.Y. Li, F.B. Su, H-K. Luo, L.Y. Liang and B. Tan, Hypercrosslinked microporous polymer networks for effective removal of toxic metal ions from water, *Micropor. Mesopor. Mater.*, 2011, 138, 207–214.

18 S. Lou and D.L. Di, Synthesis of resins with ionic liquids for purification of Flavonoids from Hippophae rhamnoides L. Leaves, *J. Agric. Food. Chem.*, 2012, 60, 6546–6558.

19 M. L. Zhang, X. J. Liang, S. X. Jiang and H. D. Qiu, Preparation and applications of surface-confined ionic-liquid stationary phases for liquid chromatography, *Trends Anal. Chem.*, 2014, 53, 60–72.

20 H.D. Qiu, M. Takafuji, X. Liu, S.X. Jiang and H. Ihara, Investigation of π-π and ion-dipole interactions on 1-allyl-3-butylimidazolium ionic liquid-modified silica stationary phase in reversed-phase liquid chromatography, *J. Chromatogr. A.*, 2010, 1217, 5190–5196.

21 X.Y. Wu, Y. Liu, Y.F. Liu and D.L. Di, Evaluation on the adsorption capability of chemically modified macroporous adsorption resin with ionic liquid, *Colloids and Surfaces A: Physicochem. Eng. Aspects.*, 2015, 469, 141–149.

22 S. M. Chacko, P. T. Thambi, R. Kuttan and I. Nishigaki, Beneficial effects of green tea: a literature review, *Chin. Med.*, 2010, 5, 1–9.

23 L. M. Sun, C. L. Zhang and P. Li, Characterization, Antimicrobial activity, and mechanism of a high-Performance (-)-epigallocatechin-3-gallate(EGCG)-Cu II/polyvinyl alcohol (PVA) nanofibrous membrane, *J. Agric. Food. Chem.*, 2011, 59, 5087–5092.

24 J.H. Huang, X.Y. Jin and S.G. Deng, Phenol adsorption on an N-methylacetamide-modified hypercrosslinked resin from aqueous solutions, *Chem. Eng. J.*, 2012, 192, 192–200.

25 C.P. Wu, C.H. Zhou and F.X. Li, Experiments of Polymeric Chemistry, Anhui Science and Technology Press, Hefei, 1987.

26 Y.F. Liu, Q.Q. Bai, S. Lou, D.L. Di, J.T. Li and M. Guo, Adsorption characteristics of (-)-epigallocatechin gallate and caffeine in the extract of waste tea on macroporous adsorption resins functionalized with chloromethyl, amino, and phenylamino groups, *J. Agric. Food. Chem.*, 2012, 60, 1555–1566.

27 M.P. Tsyurupa and V.A. Davankov, Porous structure of hypercrosslinked polystyrene: state-of-the-art mini-review, *React. Funct. Polym.*,

2006, 66, 768–779.

28 P. K. Tripathi, M.X. Liu, Y.H. Zhao, X.M. Ma, L.H. Gan, O. Noonan and C.Z. Yu, Enlargement of uniform micropores in hierarchically ordered micro–mesoporous carbon for high level decontamination of bisphenol A, *J. Mater. Chem. A.*, 2014, 2, 8534–8544.

29 J.H. Huang, G. Wang and K.L. Huang, Enhanced adsorption of salicylic acid onto a β-naphthol-modified hyper-cross-linked poly(styrene-co-divinylbenzene) resin from aqueous solution, *Chem. Eng. J.,* 2011, 168, 715–721.

30 V. Pino and A. M. Afonso, Surface-bonded ionic liquid stationary phases in high-performance liquid chromatography-A review, *Anal. Chim. Acta.*, 2012, 714, 20–37.

31 H.D. Qiu, A.K. Mallik, M. Takafuji, X. Liu, S.X. Jiang and H. Ihara, A new imidazolium-embedded C_{18} stationary phase with enhanced performance in reversed-phase liquid chromatography, *Anal. Chim. Acta.*, 2012, 738, 95–101.

32 M. Arshadi, F. SalimiVahid, J. W. L. Salvacion and M. Soleymanzadeh, Adsorption studies of methyl orange on an immobilized Mn-nanoparticle: kinetic and thermodynamic, *RSC Adv.*, 2014,4, 16005–16017.

33 Y. Liu, G.J. Cui, C. Luo, L. Zhang, Y.P. Guo and S.Q. Yan, Synthesis, characterization and application of amino-functionalized multi-walled carbon nanotubes for effective fast removal of methyl orange from aqueous solution, *RSC Adv.*, 2014, 4, 55162–55172.

34 Y.N. Chen, M.F. He, C.Z. Wang and Y.M. Wei, A novel polyvinyltetrazole-grafted resin with high capacity for adsorption of Pb(II), Cu(II) and Cr(III) ions from aqueous solutions, *J. Mater. Chem. A.*, 2014, 2, 10444–10453.

35 F.Y. Ye, R.J. Yang, X. Hua, G.H. Zhao, Adsorption characteristics of rebaudioside A and stevioside on cross-linked poly(styrene-co-divinylbenzene) macroporous resins functionalized with chloromethyl, amino and phenylboronic acid groups, *Food Chem.*, 2014, 159, 38–46.

36 A. Negrea, M. Ciopec, L. Lupa, C. M. Davidescu, A. Popa, G. Ilia and P. Negrea, Removal of As^{V} by Fe^{III}-Loaded XAD7 impregnated resin containing di(2-ethylhexyl) phosphoric ccid (DEHPA): equilibrium, kinetic, and thermodynamic modeling studies, *J. Chem. Eng. Data.*, 2011, 56, 3830–3838.

37X.T. Sun, L.G. Yang, H.F. Xing, J.M. Zhao, X.P Li, Y.B. Huang and H.Z. Liu, High capacity adsorption of Cr(VI) from aqueous solution using polyethylenimine-functionalized poly(glycidyl methacrylate) microspheres, *Colloids Surf. A: Physicochem. Eng. Aspects.*, 2014, 457, 168–169.

38 H.Y. Zhang, A.M. Li, J. Sun and P.H. Li, Adsorption of amphoteric aromatic compounds by hyper-cross-linked resins with amino groups and sulfonic groups, *Chem. Eng. J.*, 2013, 217, 354–362.

39 J.H. Huang, Molecular sieving effect of a novel hyper-cross-linked resin, *Chem. Eng. J.*, 2010, 165, 265–272.

Graphic:

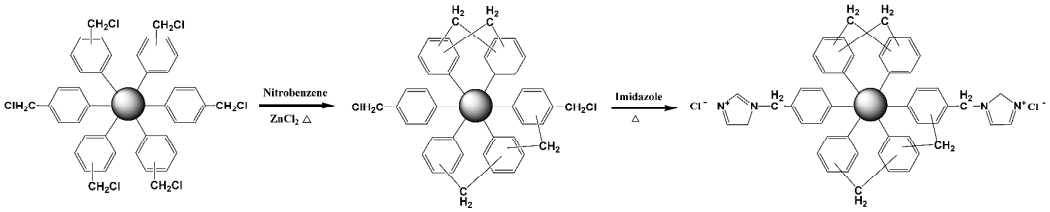

Text: Ionic liquid modified hypercrosslinked polymeric resins was synthesized and its adsorptive characteristics for catechin were studied.